arXiv:2203.00030v1 [eess.IV] 28 Feb 2022

Spatio-temporal Vision Transformer for Super-resolution Microscopy

CHARLES N. CHRISTENSEN[1,2], MENG LU[1], EDWARD N. WARD[1], PIETRO LIO[2], AND CLEMENS F. KAMINSKI[1,*]

[1] University of Cambridge, Department of Chemical Engineering and Biotechnology, Laser Analytics Group, Cambridge, UK
[2] University of Cambridge, Department of Computer Science and Technology, Artificial Intelligence Group, Cambridge, UK
[*] Corresponding author: cfk23@cam.ac.uk. – Interactive implementation and source code: http://vsr-sim.github.io

(Dated: March 2, 2022)

Structured illumination microscopy (SIM) is an optical super-resolution technique that enables live-cell imaging beyond the diffraction limit. Reconstruction of SIM data is prone to artefacts, which becomes problematic when imaging highly dynamic samples because previous methods rely on the assumption that samples are static. We propose a new transformer-based reconstruction method, VSR-SIM, that uses shifted 3-dimensional window multi-head attention in addition to channel attention mechanism to tackle the problem of video super-resolution (VSR) in SIM. The attention mechanisms are found to capture motion in sequences without the need for common motion estimation techniques such as optical flow. We take an approach to training the network that relies solely on simulated data using videos of natural scenery with a model for SIM image formation. We demonstrate a use case enabled by VSR-SIM referred to as rolling SIM imaging, which increases temporal resolution in SIM by a factor of 9. Our method can be applied to any SIM setup enabling precise recordings of dynamic processes in biomedical research with high temporal resolution.

1. INTRODUCTION

Optical microscopy is limited by the diffraction of light occurring in the optics of imaging systems. For visible light, the diffraction limit, also known as the Abbe resolution limit [1], is around 200 nm laterally. Structured illumination microscopy (SIM) is an optical microscopy technique that can achieve a two-fold spatial resolution improvement, thus enabling sub-diffraction limit imaging – a regime important for biomedical imaging [2]. Furthermore, SIM is live-cell compatible as it can be performed at relatively low excitation power. A significant challenge in applying SIM, however, remains the computational reconstruction of the acquired data into super-resolved images. The reconstruction problem in SIM is an inverse problem similar to deconvolution [3] but makes use of shifted high frequency information. The frequency-shifted signals are obtained by illuminating the sample with a temporal sequence of illumination patterns, generally sinusoidal fringes with varying orientations and phase shifts, and an image is captured for each respective pattern.

The collection of SIM images corresponding to the sequence of illumination patterns, typically a stack of 9 frames, is then used to reconstruct a super-resolved

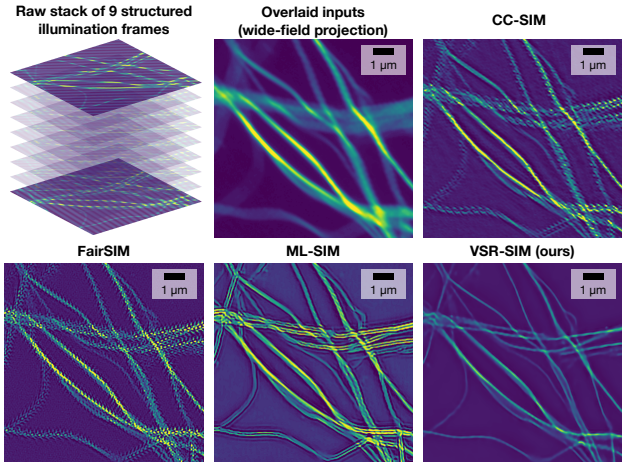


Fig. 1. Structured illumination microscopy image sequences of dynamic samples give rise to motion artefacts when previous reconstruction methods are used such as cross-correlation SIM (CC-SIM) [4], FairSIM [5] and ML-SIM [6]. The input image stack is experimental data of imaged microtubules.

image. Since SIM image stacks can be recorded at high frame rates, it is possible to image highly dynamic phenomena sequentially [7, 8]. However, the reconstruction methods that are most widely used do not make use of the temporal dimension of the acquired data [4, 5, 9, 10], because the standard semi-analytical Fourier formalism for reconstruction assumes a static sample. Hence, motion of the sample between acquired frames manifests as motion blur and reconstruction artefacts – see Fig. 1.

Deep learning offers an effective way to achieve motion compensation for video super-resolution (VSR). Recent studies demonstrate reconstruction of SIM images using neural networks [11–13], offering advantages such as improved speed and robustness to noise, but none of these reconstruction methods make use of the temporal dimension of the live-cell data. To obtain a spatio-temporal reconstruction method for SIM, we identify the following two problems that need to be overcome: (a) ground truth data for supervised learning will inherit motion blur if the targets are obtained from traditional reconstruction methods; (b) regular motion estimation methods do not work accurately on SIM data. Machine learning implementations for SIM reconstruction generally use as ground truth data a collection of carefully performed reconstructions from traditional methods, which relies on an analytical framework that assumes static samples, thus causing motion artefacts to manifest in the training data. As for (b), a common way to incorporate high-level reasoning about motion and occlusion in a model is bidirectional optical flow. However, such algorithms are not directly suited for SIM imaging, because the illumination patterns in the raw data prevent accurate calculation of motion – the varying patterns tend to be confused with motion of the subject as illustrated on Fig. 2.

We propose a method to address these two problems by building upon recent advances in using neural networks for SIM reconstruction and video super-resolution. We generalise the approach to supervised learning proposed in our previous method ML-SIM [6], in which SIM image formation is modelled to obtain synthetic training data. Instead of simulating SIM image data using static images, we use video sequences instead, which facilitates the learning of motion compensation. Instead of simulating SIM image data using static images, we use video sequences instead, such that the training data can facilitate the learning of motion compensation. To address (b), we propose a 3D transformer network architecture that solely relies on attention mechanism rather than optical flow to handle subject motion. Our contributions are three-fold:

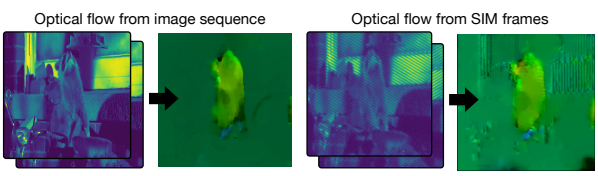


Fig. 2. Optical flow computed from video-rate SIM data leads to artefacts that are problematic for standard motion compensation techniques.

- We demonstrate a new approach to synthesising training data for machine learning models to learn spatio-temporal SIM reconstruction, in which SIM image formation is simulated using video data sequences as inputs. This enables models to be optimised for highly dynamic sequential live-cell SIM data.

- We propose a video super-resolution transformer architecture that uses shifted windows with 3-dimensional patches to capture the spatio-temporal correlations in live-cell SIM data with windowed multi-head attention. We introduce residual connections between transformer blocks with channel attention as an additional attention mechanism.

- We showcase a unique application of our method, rolling SIM imaging, where a moving window of frames is used for reconstruction. Our reconstruction method lends itself particularly well to rolling SIM imaging because it can be recast as a video super-resolution problem, where the reconstruction of each SIM stack uses SIM frames from the previous and subsequent SIM stack acquisition. This increases the temporal resolution of SIM imaging by a factor of 9, enabling dynamic processes in biomedical research to be resolved without the motion artefacts that plague previous methods.

An online, ready-to-use and interactive implementation can be found at http://vsr-sim.github.io. Source code, datasets and trained models are provided at http://github.com/charlesnchr/vsr-sim.

2. RELATED WORK

Optical super-resolution microscopy. Optical super-resolution microscopy techniques have emerged over the last three decades to now form an essential tool for medical imaging. Several semi-analytical methods have been proposed for SIM reconstruction [4, 5, 9, 14–16], e.g. FairSIM and OpenSIM. These methods rely on Fourier transformations, Wiener filters and iterative deconvolution, which can induce honeycomb and ringing artefacts, especially when noise and motion blur are significant [17]. Multiple machine learning implementations for SIM reconstruction have been proposed in the past year [6, 12, 13] based on convolutional neural networks that take in SIM stacks and output super-resolved images. Two such examples are U-Net-SIM [12] and ML-SIM [6] using U-Net [18] and RCAN [19] backbones, respectively. These methods offer reconstruction with fewer frames, higher processing speed and increased robustness to noise compared to Fourier methods. None of these studies considered fast-moving samples. In [20], however, SIM is applied to image highly dynamic samples using a semi-analytical reconstruction method. This is achieved using rolling SIM imaging, as further explored in Sec. D, with a very short exposure time, such that motion artefacts can be minimised. This can lead to high frame rates, but at a significant loss of image quality, i.e. low signal-to-noise ratio from which spatial resolution decreases. This trade-off between temporal and spatial resolution is prevalent in the field

because none of the existing reconstruction methods for SIM exploits the spatio-temporal nature of live-cell data. Applications of existing methods may only reduce motion artefacts via this trade-off, whereas the capability to perform motion compensation during reconstruction would handle these artefacts directly while maintaining image quality.

Image and video super-resolution. Methods using convolutional neural networks as a backbone have long been state-of-the-art for image and video super-resolution (SR). Dong *et al*. pioneered the pursuit of learning-based methods for image SR by achieving superior performance to traditional methods using a CNN with only three layers [21]. A similar network for VSR was proposed by Kappeler et al. [22]. With the emergence of residual networks [23], it became possible to build deeper networks. Ledig *et al*. repurposed ResNet for SR with the network SRResNet [24]. An attention mechanism was introduced by Zhang *et al*. [25] with residual channel attention network (RCAN) becoming a new state-of-the-art method. More recently, multi-head attention has been introduced for SR using transformer-based architectures with IPT [26] and SwinIR [27].

For VSR, the spatio-temporal correlations between input frames are essential to model for optimal performance. Most VSR methods use frame alignment enabled by motion estimation and compensation [28]. For motion estimation, a popular approach is using optical flow [29]. A state-of-the-art VSR method that uses optical flow is RBPN [30], which is based on a recurrent CNN architecture. Recently, the method BurstSR [31] was proposed for SR reconstruction of images taken in quick succession with a handheld camera. The problem is similar in principle to SIM reconstruction, but the method is not directly applicable as it is based on optical flow for alignment. Methods that do not use optical flow tend to rely on 3D convolutional networks [32, 33]. However, Choi *et al*. demonstrated that channel attention as a sole mechanism is a strong baseline for motion compensation in the related problem of video interpolation [34].

Vision transformer. With the advent of Vision Transformer (ViT) [35], transformer networks are beginning to replace CNNs for low-level computer vision tasks. ViT introduced multi-head self-attention (MSA) for image input, which proves to be a very flexible mechanism for vision, but does require a substantial number of trainable parameters compared with equivalently performing CNNs. Liu *et al*. demonstrated that using a hierarchy of shifted window MSA modules, their proposed transformer architecture, Swin, can incorporate the large receptive field of ViT, while having the same efficient inductive bias that CNNs offer [36]. Variations of the Swin transformer have become state-of-the-art in image restoration, SwinIR [27], and video classification [33].

3. DATA GENERATION

Acquiring a real pairwise dataset for supervised learning in the context of super-resolution microscopy is problematic. Experimentally, the ground truths cannot be obtained, which leaves the options of using either the output from traditional reconstruction methods as a target [13, 37] or a different optical super-resolution modality [38]. The former approach prevents the method from generalising and improving beyond traditional methods, and the latter is highly prone to artefacts, while not being live-cell compatible. Therefore, we take the approach of generating a synthetic dataset using a SIM image formation model [6] on a video dataset, which provides ideal ground truths and diverse training data.

Test sets	Motion regime			
	Static	Medium	Fast	Extreme
Source	DIV2K	BBC	REDS	REDS
Data type	Image	Video	Video	Video
Frame skip	-	No	No	Yes
Samples #	200	50	10	10
Max flow	0	10.2	27.3	46.2
Median flow	0	1.5	10.4	18.1

Table 1. The four test sets that have been prepared for experiments using the source datasets DIV2K [39], a subset of our BBC video dataset, and REDS [40]. The motion is amplified by skipping every other frame for the Extreme test set. Motion is quantified by calculating max and median of the magnitude of optical flow between the first and center frame in all sequences for a dataset at 512x512 resolution.

Video dataset. Inspired by DIV2K [39] for SISR, we built a large video dataset focusing on diversity and high-resolution footage. Specifically, this dataset is designed to have targets of at least 1024x1024 pixels to make the image formation model more consistent with typical experimental data from SIM systems, thus facilitating model inference performance. Many previous VSR datasets are limited in scope and are intended for video classification [41, 42] or more suitable for testing, e.g. REDS [40], while others only have a small subset of high-resolution, diverse data, e.g. Vimeo90k [43]. Our dataset consists of 200 hours of high-quality footage from nature documentaries produced by the BBC. Samples are included here with permission and video data has been obtained under the ERA License. The collection of videos is sampled to generate 100,000 image sequences, each consisting of 9 frames. A subset is reserved for testing, for which we also use DIV2K and REDS. The DIV2K dataset is a single image dataset, and with the image formation model described in the following paragraph, these still images correspond to imaging static subjects. The REDS dataset features videos recorded with a handheld camera with a high level of image translation from frame to frame. To make the motion in the REDS video even more extreme, we prepared an extra test set by sampling the videos with frame skipping, such that only every second frame was kept. These datasets were used to prepare four test sets to assess reconstruction performance in different motion regimes. The difficulty associated with a dataset depends on the level of motion that its samples exhibit. We quantify this using the mean

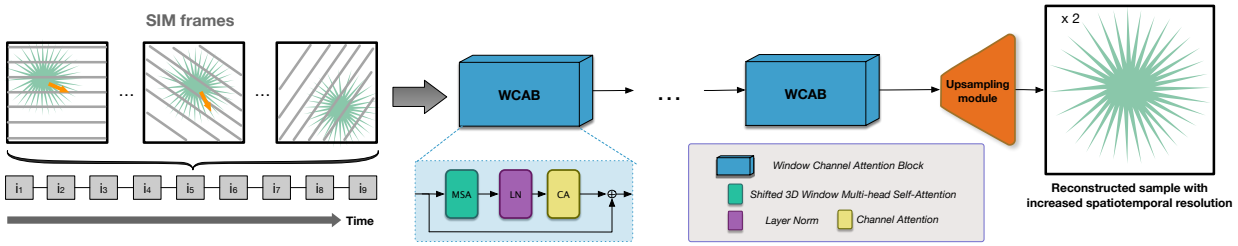


Fig. 3. Architecture of the proposed windowed channel attention network. Skip connections are added between the attention blocks in a similar fashion to residual networks.

and maximum value of optical flow magnitude averaged over all samples in the respective datasets. See Tab. 1 for further specification. Further details on the dataset sampling is provided in Supplementary.

Image formation model. SIM enables optical super-resolution by encoding structural details corresponding to high spatial frequencies of the sample into signals in the lower frequency domain. By unmixing the low-frequency data, information can then be recovered that would otherwise be lost with conventional wide-field imaging. The diffraction limit is described by the optical transfer function (OTF), which represents the transmittable bandwidth of spatial frequency through an imaging system. It is by shifting high spatial frequencies into the accessible passband that super-resolution by SIM is obtained. The OTF is the Fourier transform of the point spread function (PSF), which is the blur kernel in direct space. Conventional wide-field SIM uses sinusoidal illumination patterns formed by the interference of two beams [14]. The illumination pattern has an orientation and a phase shift, which are typically varied over 3 values to ensure symmetric frequency support, thus leading to a stack of 9 frames with different patterns. In mathematical terms, SIM reconstruction solves the inverse problem of this excitation and blurring operation, thus determining the fluorescent signal that represents the sample.

The ideal OTF is generated based on a given objective numerical aperture, pixel size and fluorescence emission wavelength. The illumination stripe patterns are calculated from their spatial frequency k_0 and phase ϕ,

$$I_{\theta,\phi}(x,y) = I_0\left[1 - \frac{m}{2}\cos\left(2\pi(k_x x + k_y y) + \phi\right)\right], \quad (1)$$

where k_x, $k_y = k_0\cos\theta$, $k_0\sin\theta$ for a pattern orientation θ relative the horizontal axis, ϕ defines the phase of the pattern (i.e. the lateral shift in the direction of k_0) and m is the modulation depth, which defines the relative strength of the super-resolution information contained in the raw images. The fluorescent response of the sample can then be modelled by the multiplication of the sample structure, $S_t(x,y)$, i.e. input image, at time t and the illumination pattern intensity $I_{\theta,\phi}(x,y)$. The final image, $D_{t,\theta,\phi}(x,y)$, is formed after blurring by the PSF, $H(x,y)$, and addition of white Gaussian noise, $N(x,y)$,

$$D_{t,\theta,\phi}(x,y) = \left[S_t(x,y)I_{\theta,\phi}\right] \otimes H(x,y) + N(x,y), \quad (2)$$

where $\otimes$ is the convolution operation. The set of sampled images from a sequence in the video dataset corresponds to the time points $t \in [1,9]$. A full SIM stack is comprised of the set $\left\{D_{t,\theta,\phi} \mid t \in [1,9]\right\}$, where each value of t is associated with a distinct illumination pattern, i.e. a unique permutation of θ and ϕ. Each consecutive 9 frames then contain a full cycle of illumination patterns. In addition to Gaussian noise, added pixel-by-pixel, a random error is added to the parameters for the stripe patterns, k_0, θ and ϕ, to approximate the inherent uncertainty in an experimental setup for illumination pattern generation as well as forcing the model to generalise when learning the reconstruction task from the data. Poisson noise can further be introduced to more realistically approximate the noise sources present in experimental data. For implementation details and specification of optical parameters see Supplementary.

4. MODEL ARCHITECTURE

The proposed model is inspired by the vision transformer network [35] in particular its more efficient shifted window variant, Swin [36], with its extension for video classification, Video Swin [33], and adaption to image restoration, SwinIR [27]. Swin introduced the inductive bias to self-attention called shifted window multi-head attention (SW-MSA), which can be compared to the inductive bias inherent to convolutional networks. SwinIR introduced residual blocks to the Swin transformer to help preserve high-frequency information for deep feature extraction. The Video Swin transformer generalised the SW-MSA to three dimensions, such that spatio-temporal data can be included in the local attention for the self-attention calculation. Further to this, the success of the channel attention mechanism in [25] inspires the inclusion of this other inductive bias in addition to 3D local self-attention following the SW-MSA approach.

The inputs to the model have dimension $T \times H \times W \times C$, where T is 9 for SIM reconstruction and C is 1. A shallow feature extraction module in the beginning of the network architecture Fig. 3 projects the input into a feature map, F_0, of $T \times H \times W \times D$ dimension, where the embedding dimension, D, is a hyperparameter. The feature map is passed through a sequence of residual blocks, denoted Window Channel Attention Block (WCAB)

$$F_i = H_{\text{WCAB}}(F_{i-1}), \quad i = 11, .., n \quad (3)$$

Inside each WCAB is a sequence of Swin Transformer Layers (STLs), in which multi-head self-attention is calculated using local attention with shifted window mechanism. Inputs to STL layer is partitioned into $\frac{T}{P} \times \frac{HW}{M^2}$

3D tokens of $P \times M^2 \times D$ dimension. For a local window feature, $x \in \mathbb{R}^{P \times M^2 \times D}$, query, key and value matrices, $\{Q, K, V\} \in \mathbb{R}^{PM^2 \times D}$, are computed by multiplication with projection matrices following the original formulation of transformers [44]. Attention is then computed as

$$\text{Attention}(Q, K, V) = \text{SoftMax}(QK^T/\sqrt{d} + B)V, \quad (4)$$

where $B \in \mathbb{R}^{P^2 \times M^2 \times M^2}$ is a relative positional bias found to lead to significant improvements in [36]. STLs are joined in a way similar to the residual blocks, although the use of SW-MSA is alternated with a version without shifted windows, W-MSA, ensuring that attention is computed across window boundaries, which would not have been the case without SW-MSA.

After the final STL, the m-th layer, in a WCAB, a transposed 3-dimensional convolutional layer is used to project the 3D tokens back into a $T \times H \times W \times D$ feature map, $F_{i,m}$. A channel attention module is then used on $F_{i,m}$ to determine the dependencies between channels following the calculation of the channel attention statistic [25]. The mechanism works by using global adaptive average pooling to reduce the feature map to a vector which after passing through a 2D convolutional layer becomes weights that are multiplied back onto $F_{i,m}$, such that channels are adaptively weighed. A residual is then obtained by adding a skip connection from the beginning of the i-th WCAB to prevent loss of information, i.e. low-frequency information, and the vanishing gradient problem. A fusion layer combines the temporal dimension and the channel dimensions. For the final upsampling module, we use the sub-pixel convolutional filter [45] to expand the image dimensions by aggregating the fused feature maps. The implementation will be made available on Github and is provided in the Supplementary.

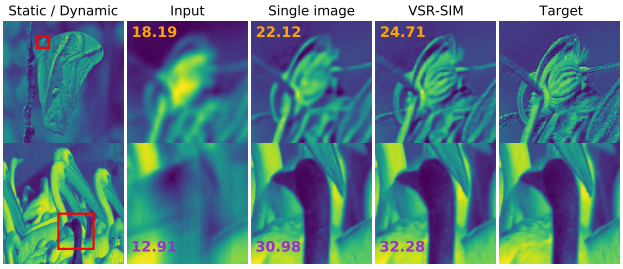


Fig. 4. For static subjects (top row) the method defaults to standard SIM reconstruction, which offers significant improvements over a deconvolution baseline trained with the same architecture. For dynamic input data (bottom row), the advantage of SIM diminishes depending on the level of motion, but, importantly, VSR-SIM does not generate motion artefacts in this setting.

5. EXPERIMENTS

Implementation details. All models described in the following were trained using the Adam optimiser and a mean squared error loss function with a learning rate of 1e-4 that is halved every 100,000 iterations. A total of 500,000 iterations were made, which equals 5 epochs of the BBC training dataset. A set of 4 Nvidia A100 GPUs was used with a batch size per GPU of 4. Training samples were randomly cropped to 128x128 inputs and 256x256 targets, while inference was performed with 512x512 inputs resulting in 1024x1024 outputs. For VSR-SIM, the WCAB number, STL number, window size, embedding size D and attention head number are set to 6, 6, 8, 96 and 6, respectively. The hyperparameters of the other tested architectures follow original implementations and are further specified in Supplementary.

Reconstruction method	Test set (PSNR)	
	Static	Medium
Wide-field baseline	22.79	17.31
CC-SIM [4]	27.99	16.98
OpenSIM [9]	28.34	14.04
FairSIM [5]	28.54	15.34
ML-SIM [6]	32.30	18.41
VSR-SIM (ours)	**34.74**	**30.15**

Table 2. Synthetic test sets were evaluated with four existing SIM reconstruction methods and VSR-SIM. The static test set was generated using still images from DIV2K [39] and the dynamic test set was generated using image sequences sampled from the BBC video dataset. At high levels of motion, other SIM reconstruction methods fail, but VSR-SIM can maintain a high reconstruction quality for the dynamic test set.

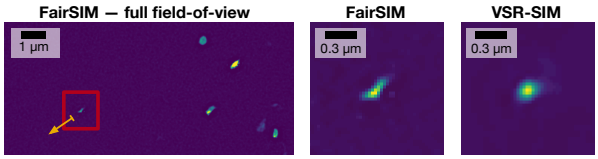


Fig. 5. Lysosome, a spherical vesicle, moving rapidly in a sample of COS-7 cells. FairSIM is unable to handle motion blur and reconstructs an elongated shape, while VSR-SIM reconstructs a circular shape consistent with the known shape of the lysosome.

A. Comparison with state-of-the-art

SIM reconstruction methods. The Static and Medium test sets, see Tab. 1 for details, were evaluated with our method, VSR-SIM, and four existing SIM methods: CC-SIM [4], OpenSIM [9], FairSIM [5] and ML-SIM [6]. The results are listed in Tab. 2 based on peak signal-to-noise ratio (PSNR). For the Static test set the difference in reconstruction quality is relatively even, but for the Medium test set, most previous methods fail to surpass the diffraction-limited wide-field baseline. This is due to motion artefacts and inaccurate numerical optimisation (e.g. parameter estimation using peak finding in the case of FairSIM) becoming substantial. An example illustrating motion artefacts in reconstruction output for an

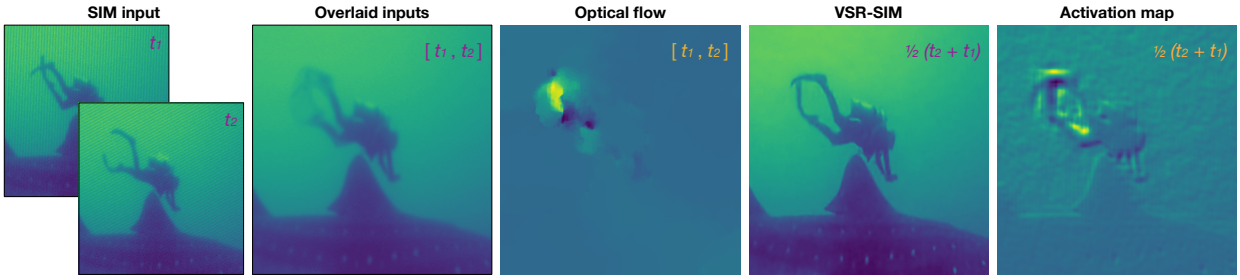


Fig. 6. Self-attention appears to emphasise the regions, in which motion occurs. The activations from the final attention heads are found to be well correlated with intensity maps of optical flow.

Method	Test set (PSNR)			
	Static	Medium	Fast	Extreme
Bicubic†	26.40	26.35	22.63	21.08
SISR†	31.23	28.08	25.38	22.50
VSR†	31.15	28.15	25.41	**22.98**
VSR-SIM	**34.74**	**30.15**	**26.04**	22.95
RBPN	33.16	29.25	25.29	21.48
Wide-field	26.24	22.99	19.32	18.77

Table 3. Test of our method in different motion regimes compared with baseline models trained and evaluated using input without structured illumination. Methods denoted with † are based on input without illumination patterns. The SISR and VSR baseline methods use the same architecture as VSR-SIM. The sub-diffraction limit resolution of SIM is achievable despite significant motion in the input data, but is ultimately lost for an extreme level of motion. RBPN that uses optical flow for motion estimation was not found to perform comparably, suggesting that optical flow is not needed.

CA	SW-MSA	3D window	Score (PSNR)
✓			29.06
	✓		29.48
	✓	✓	29.10
✓	✓		30.01
✓	✓	✓	**30.15**

Table 4. Ablation study on the inclusion of different attention mechanisms. CA is channel attention [25], SW-MSA [36] and 3D window refers to 3D window attention for spatio-temporal data [33]. The scores are based on evaluations on the Medium test set.

input sample with significant motion is shown in Fig. 1.

We tested the spatio-temporal resolution of reconstruction on a real sample by imaging fast-moving lysosomes within the endoplasmic reticulum (ER) in COS-7 cells [46]. We use the SiR-lysosome fluorophore with an excitation wavelength of 652 nm. Given the same raw data, we observe differences in the shape of the lysosome following reconstructing with FairSIM and VSR-SIM, see Fig. 5. FairSIM produces an elongated shape suggesting that motion blur is reconstructed into features, which is further supported by the simulated test in Sec. C.

B. Ablation study

No structured illumination patterns. An important baseline for SIM reconstruction is deconvolution, which in this context is considered a deblurring operation that does not need patterned illumination. A single-image deconvolution method is useful for wide-field imaging to counter the effect of the PSF and noise sources, but it cannot provide optical SR. We trained a model with the same architecture as VSR-SIM using an equivalent dataset without illumination patterns to synthesise wide-field images. On Fig. 4, example output can be seen showing the SISR baseline model versus VSR-SIM that takes SIM input. In the first input sample, the subject is static, and the quality difference of the outputs is significant. For more dynamic subjects, the difficulty of the SIM reconstruction problem increases, and the difference to the SISR baseline is smaller. We explored this further by testing models on the four test sets shown in Tab. 1. The four test sets are evaluated with a deconvolution SISR baseline, a deconvolution VSR baseline, a state-of-the-art VSR method RBPN [30] and our method VSR-SIM. The two baseline models are based on the VSR-SIM architecture but trained and tested without illumination patterns, while RBPN and VSR-SIM are trained with SIM inputs. Only the center frame in a sequence corresponding to the target is input to the SISR model, whereas the VSR model works on the full image sequence. The test results in Tab. 3 show that VSR-SIM enables high-quality SIM reconstruction in every motion regime. The quality of the reconstruction outputs is markedly better than for the baselines in all but the most extreme case with frame skipping. Hence, at very high levels of motion, the SIM modality does not offer an advantage over conventional imaging. This is consistent with previous theoretical findings of Ströhl and Kaminski [47].

Optical flow. As illustrated in Fig. 2 the determination of optical flow can be hindered by the presence of an illumination pattern. The quantitative impact of including optical flow is tested by training RBPN, which uses optical flow for inputting aligned frames into a recurrent network in a mechanism called back-projection. In Tab. 3 it is found that the VSR-SIM model outperforms RBPN in

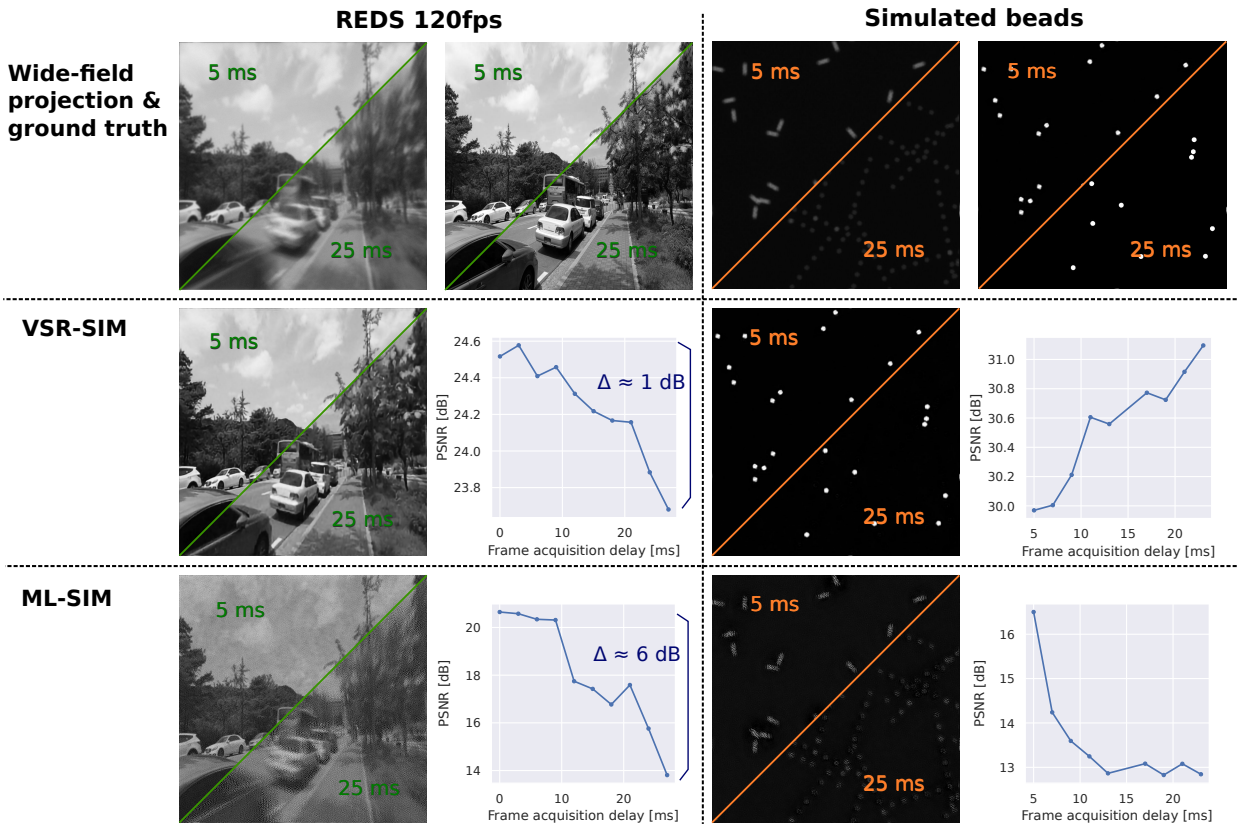


Fig. 7. Reconstruction performance for VSR-SIM does not collapse for inputs that exhibit significant levels of motion. Given the same inputs sequences, the motion can be controlled via a set delay between frames. This is done with frame skipping for a high frame rate video sequence, REDS 120fps [40], and sequences of simulated beads.

different motion regimes although it does not use optical flow. This indicates that the two attention mechanisms of VSR-SIM are sufficient to attend to regions that exhibit a lot of motion. This is further explored by visualising the activation maps from the final attention heads in the network, see Fig. 6. Comparing the two frames for t_1 and t_2, it is clear that the motion in this sequence occurs in a very specific region, which is picked up by the optical flow intensity projection as well as the activation map.

Attention mechanisms. The respective importance of multi-head self-attention, 3D window attention and channel attention is investigated by training different variants of the model on the same training dataset and testing it with our Medium test set. The results are summarised in Tab. 4. The most significant mechanism according to these results is the multi-head self-attention, which is implemented in a similar way to SwinIR [27] when 3D window attention is excluded.

C. Speed limit of SIM reconstruction

As indicated in Table Tab. 3, the reconstruction quality of VSR-SIM approaches that of a similarly trained deconvolution method, meaning that the sub-diffraction imaging enabled by SIM becomes increasingly difficult to achieve as the motion increases. Importantly, however, since VSR-SIM is trained on SIM video data spanning multiple motion regimes, the case of extreme motion does not cause the method to collapse and perform significantly worse than the deconvolution baseline. We investigate this ability further by reconstructing inputs that have variable delay between frames and comparing the results to those of ML-SIM, which has no capability to handle motion. As the input data we sample from a high frame rate video sequence from Reds [40] and generate images of moving simulated beads. The results are shown on Fig. 7. Although the performance decreases as the frame delay increases, the drop is much smaller than for ML-SIM; namely 1 dB versus 6 dB over the range of 0-25 ms frame delay in case of the video sequence from Reds. In case of the simulated beads, the performance does not decrease. This indicates that VSR-SIM is able to ignore the adjacent frames in a SIM stack if the motion is high enough, which presumably becomes easier for the

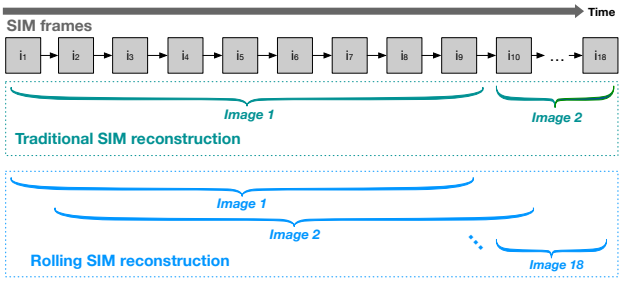


Fig. 8. Rolling SIM imaging scheme for structured illumination microscopy, which is utilised in the proposed method.

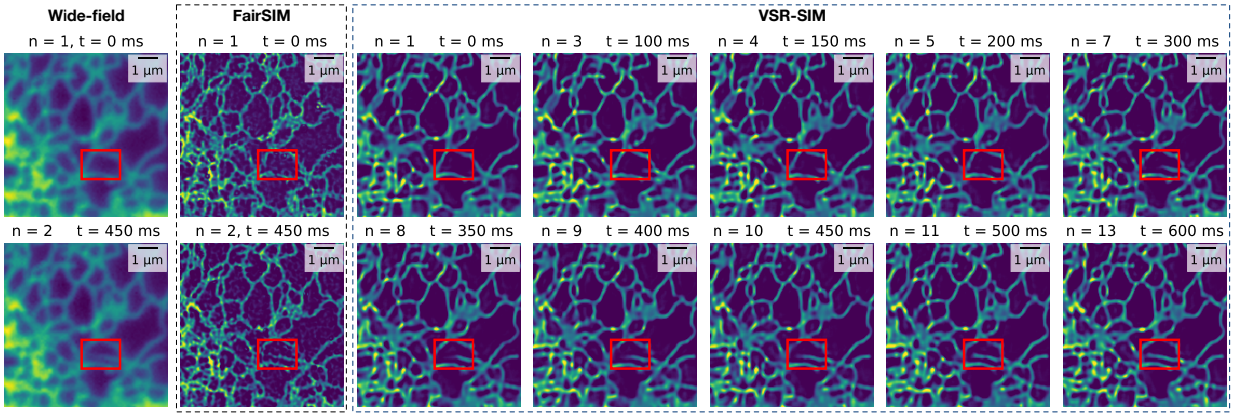


Fig. 9. Our method, VSR-SIM, and the widely used method FairSIM applied to a SIM image sequence of the endoplasmic reticulum. Both methods offer significant improvements over wide-field imaging. The rectangle emphasises a reshaping event of a tubule. Compared with FairSIM, our method achieves 9 times higher temporal resolution by enabling the rolling SIM imaging scheme, see Fig. 8. The spatial resolution of FairSIM is higher, but the data contains more artefacts.

model to do as the spatial separation between the beads increases.

D. Rolling SIM algorithm

When performing SIM reconstruction with conventional methods, the order of illumination patterns in a stack has to be consistent across stacks. To increase the temporal resolution of SIM, one can use frames that belong to adjacent stacks, thus having a rolling window for which frames are included in the current stack, which reduces the number of frames to be acquired per individual stack. This scheme for SIM imaging is illustrated in Fig. 8. In the scheme depicted here, the rolling window is shifting by a single frame at a time, therefore increasing the temporal resolution by a factor of 9. To reconstruct SIM frames according to a rolling window, the reconstruction method must be able to handle inputs with varying order of illumination patterns. We address this by shuffling illumination patterns for every training sample that is generated for the training data. The shuffling is without replacement such that a complete cycle is always present in an input. This approach forces the model to learn to handle arbitrary orderings facilitating the rolling SIM scheme. Combined with the motion compensating reconstruction method that can work at motion regimes that traditionally would be unmanageable, imaging at high speed with high granularity becomes possible. This capability lends itself well to applications with fast-moving samples that exhibit intricate movement behaviour. The scheme can similarly be applied for long-term imaging by utilising the higher photon efficiency coming with acquiring only a single frame per reconstructed output.

Improving temporal resolution. To demonstrate our model applied to the rolling SIM scheme, we performed an experiment imaging endoplasmic reticulum in COS-7 cells, labelled with the sec61-mApple and imaged with an excitation wavelength of 561 nm. The FairSIM reconstruction method [5] is used as a baseline as it is widely used in the microscopy community [48]. The endoplasmic reticulum is the largest membrane structure inside the cell and displays drastic reshaping with constant tubule elongation, retraction and junction formation as shown on Fig. 9. This dynamic reshaping is important to regulate the morphology and function of ER inside the cell. Compromised reshaping dynamics of ER is associated with a variety of diseases, including Alzheimer's disease [49], which makes it important to record, measure and understand these dynamics. On Fig. 9 an occurrence of reshaping can be seen in the area marked by the rectangle over a sequence of 20 frames each acquired with a 50 ms exposure time. Using FairSIM for the reconstruction provides only two super-resolved SIM images, rendering the reshaping event very abrupt and less noticeable. Using VSR-SIM with the rolling SIM scheme, the raw sequence leads to 19 reconstructed outputs, of which 12 are included showing a significantly more granular process. FairSIM, however, is seen to recover more high-frequency information in its two outputs indicating that it achieves a higher spatial resolution, although at the expense of more artefacts.

6. CONCLUSION

We have proposed a new transformer architecture that combines channel attention with multi-head self-attention computed using shifted 3D windows. This architecture is shown to excel at the SIM reconstruction task for dynamic inputs. A demonstration of using the method for a use case in medical research is made with implementation of rolling SIM imaging, in which a moving window of SIM frames is used for reconstruction providing a temporal resolution that is 9 times higher, while still providing comparable spatial resolution well beyond the diffraction limit. Our method can be used for any SIM imaging system as it is purely trained on synthetic data using our image formation model that can be easily adapted to different SIM configurations.

ACKNOWLEDGMENTS

CFK acknowledges funding from the UK Engineering and Physical Sciences Research Council, EPSRC

(grants EP/L015889/1 and EP/H018301/1), the Wellcome Trust (grants 3-3249/Z/16/Z and 089703/Z/09/Z) and the UK Medical Research Council, MRC (grants MR/K015850/1 and MR/K02292X/1), MedImmune, and Infinitus (China) Ltd. The Research Computing Services of the University of Cambridge enabled the high-performance computations in this work.

DISCLOSURES

Disclosures. The authors declare no conflicts of interest.

REFERENCES

1. C. W. Mccutchen, "Superresolution in microscopy and the Abbe resolution limit," JOSA **57**, 1190–1192 (1967).
2. K. Iqbal, F. Liu, C.-X. Gong, and I. Grundke-Iqbal, "Tau in Alzheimer disease and related tauopathies," Current Alzheimer Research **7**, 656–664 (2010).
3. F. Ströhl and C. F. Kaminski, "A joint richardson—lucy deconvolution algorithm for the reconstruction of multifocal structured illumination microscopy data," Methods and Applications in Fluorescence **3**, 014002 (2015).
4. K. Wicker, "Non-iterative determination of pattern phase in structured illumination microscopy using auto-correlations in Fourier space," Optics Express **21**, 24692 (2013).
5. M. Müller, V. Mönkemöller, S. Hennig, W. Hübner, and T. Huser, "Open-source image reconstruction of super-resolution structured illumination microscopy data in ImageJ," Nature Communications **7**, 10980 (2016).
6. C. N. Christensen, E. N. Ward, M. Lu, P. Lio, and C. F. Kaminski, "ML-SIM: universal reconstruction of structured illumination microscopy images using transfer learning," Biomedical optics express **12**, 2720–2733 (2021).
7. D. Holcman, P. Parutto, J. E. Chambers, M. Fantham, L. J. Young, S. J. Marciniak, C. F. Kaminski, D. Ron, and E. Avezov, "Single particle trajectories reveal active endoplasmic reticulum luminal flow," Nature cell biology **20**, 1118 (2018).
8. T. A. Planchon, L. Gao, D. E. Milkie, M. W. Davidson, J. A. Galbraith, C. G. Galbraith, and E. Betzig, "Rapid three-dimensional isotropic imaging of living cells using Bessel beam plane illumination," Nature methods **8**, 417 (2011).
9. A. Lal, C. Shan, and P. Xi, "Structured illumination microscopy image reconstruction algorithm," IEEE Journal on Selected Topics in Quantum Electronics **22**, 1–15 (2016).
10. X. Huang, J. Fan, L. Li, H. Liu, R. Wu, Y. Wu, L. Wei, H. Mao, A. Lal, P. Xi, and Others, "Fast, long-term, super-resolution imaging with Hessian structured illumination microscopy," Nature biotechnology **36**, 451–459 (2018).
11. C. N. Christensen, E. N. Ward, P. Lio, and C. F. Kaminski, "ML-SIM: a deep neural network for reconstruction of structured illumination microscopy images," arXiv preprint arXiv:2003.11064 (2020).
12. L. Jin, B. Liu, F. Zhao, S. Hahn, B. Dong, R. Song, T. C. Elston, Y. Xu, and K. M. Hahn, "Deep learning enables structured illumination microscopy with low light levels and enhanced speed," Nature communications **11**, 1–7 (2020).
13. C. Ling, C. Zhang, M. Wang, F. Meng, L. Du, and X. Yuan, "Fast structured illumination microscopy via deep learning," Photonics Research **8**, 1350–1359 (2020).
14. M. G. Gustafsson, "Surpassing the lateral resolution limit by a factor of two using structured illumination microscopy," Journal of Microscopy **198**, 82–87 (2000).
15. G. Ball, J. Demmerle, R. Kaufmann, I. Davis, I. M. Dobbie, and L. Schermelleh, "SIMcheck: a toolbox for successful super-resolution structured illumination microscopy," Scientific reports **5**, 1–12 (2015).
16. K. Wicker, O. Mandula, G. Best, R. Fiolka, and R. Heintzmann, "Phase optimisation for structured illumination microscopy," Optics Express **21**, 2032 (2013).
17. J. Demmerle, C. Innocent, A. J. North, G. Ball, M. Müller, E. Miron, A. Matsuda, I. M. Dobbie, Y. Markaki, and L. Schermelleh, "Strategic and practical guidelines for successful structured illumination microscopy," Nature Protocols **12**, 988–1010 (2017).
18. O. Ronneberger, P. Fischer, and T. Brox, "U-Net: Convolutional Networks for Biomedical Image Segmentation," (2015).
19. Y. Zhang, K. Li, K. Li, L. Wang, B. Zhong, and Y. Fu, "Image super-resolution using very deep residual channel attention networks," Tech. rep. (2018).
20. X. Huang, J. Fan, L. Li, H. Liu, R. Wu, Y. Wu, L. Wei, H. Mao, A. Lal, P. Xi, L. Tang, Y. Zhang, Y. Liu, S. Tan, and L. Chen, "Fast, long-term, super-resolution imaging with Hessian structured illumination microscopy," Nature Biotechnology **36**, 451–459 (2018).
21. C. Dong, C. C. Loy, K. He, and X. Tang, "Image Super-Resolution Using Deep Convolutional Networks," IEEE Transactions on Pattern Analysis and Machine Intelligence **38**, 295–307 (2014).
22. A. Kappeler, S. Yoo, Q. Dai, and A. K. Katsaggelos, "Video Super-Resolution With Convolutional Neural Networks," IEEE Transactions on Computational Imaging **2**, 109–122 (2016).
23. K. He, X. Zhang, S. Ren, and J. Sun, "Deep residual learning for image recognition," Proceedings of the IEEE Computer Society Conference on Computer Vision and Pattern Recognition **2016-Decem**, 770–778 (2016).
24. C. Ledig, L. Theis, F. Huszár, J. Caballero, A. Cunningham, A. Acosta, A. Aitken, A. Tejani, J. Totz, Z. Wang, and W. Shi, "Photo-realistic single image super-resolution using a generative adversarial network," Proceedings - 30th IEEE Conference on Computer Vision and Pattern Recognition, CVPR 2017 **2017-Janua**, 105–114 (2017).
25. Y. Zhang, K. Li, K. Li, L. Wang, B. Zhong, and Y. Fu, "Image super-resolution using very deep residual channel attention networks," Lecture Notes in Computer Science (including subseries Lecture Notes in Artificial Intelligence and Lecture Notes in Bioinfor-

matics) **11211 LNCS**, 294–310 (2018).
26. H. Chen, Y. Wang, T. Guo, C. Xu, Y. Deng, Z. Liu, S. Ma, C. Xu, C. Xu, and W. Gao, "Pre-Trained Image Processing Transformer," (2020).
27. J. Liang, J. Cao, G. Sun, K. Zhang, L. Van Gool, and R. Timofte, "SwinIR: Image Restoration Using Swin Transformer," (2021).
28. H. Liu, Z. Ruan, P. Zhao, C. Dong, F. Shang, Y. Liu, and L. Yang, "Video Super Resolution Based on Deep Learning: A Comprehensive Survey," (2020).
29. B. K. P. Horn and B. G. Schunck, "Determining optical flow," Artificial intelligence **17**, 185–203 (1981).
30. M. Haris, G. Shakhnarovich, and N. Ukita, "Recurrent back-projection network for video super-resolution," Proceedings of the IEEE Computer Society Conference on Computer Vision and Pattern Recognition **2019-June**, 3892–3901 (2019).
31. G. Bhat, M. Danelljan, L. Van Gool, and R. Timofte, "Deep Burst Super-Resolution," (2021).
32. Y. Jo, S. W. Oh, J. Kang, and S. J. Kim, "Deep video super-resolution network using dynamic upsampling filters without explicit motion compensation," in "Proceedings of the IEEE conference on computer vision and pattern recognition," (2018), pp. 3224–3232.
33. Z. Liu, J. Ning, Y. Cao, Y. Wei, Z. Zhang, S. Lin, and H. Hu, "Video Swin Transformer," pp. 1–12 (2021).
34. M. Choi, H. Kim, B. Han, N. Xu, and K. M. Lee, "Channel attention is all you need for video frame interpolation," AAAI 2020 - 34th AAAI Conference on Artificial Intelligence pp. 10663–10671 (2020).
35. A. Dosovitskiy, L. Beyer, A. Kolesnikov, D. Weissenborn, X. Zhai, T. Unterthiner, M. Dehghani, M. Minderer, G. Heigold, S. Gelly, J. Uszkoreit, and N. Houlsby, "An Image is Worth 16x16 Words: Transformers for Image Recognition at Scale," (2020).
36. Z. Liu, Y. Lin, Y. Cao, H. Hu, Y. Wei, Z. Zhang, S. Lin, and B. Guo, "Swin Transformer: Hierarchical Vision Transformer using Shifted Windows," (2021).
37. L. Jin, B. Liu, F. Zhao, S. Hahn, B. Dong, R. Song, T. C. Elston, Y. Xu, and K. M. Hahn, "Deep learning enables structured illumination microscopy with low light levels and enhanced speed," Nature Communications **11** (2020).
38. H. Wang, Y. Rivenson, Y. Jin, Z. Wei, R. Gao, H. Günaydin, L. A. Bentolila, C. Kural, and A. Ozcan, "Deep learning enables cross-modality super-resolution in fluorescence microscopy," Nature methods **16**, 103–110 (2019).
39. E. Agustsson and R. Timofte, "NTIRE 2017 Challenge on Single Image Super-Resolution: Dataset and Study," Tech. rep. (2017).
40. S. Nah, S. Baik, S. Hong, G. Moon, S. Son, R. Timofte, and K. M. Lee, "NTIRE 2019 Challenge on Video Deblurring and Super-Resolution: Dataset and Study," in "CVPR Workshops," (2019).
41. W. Kay, J. Carreira, K. Simonyan, B. Zhang, C. Hillier, S. Vijayanarasimhan, F. Viola, T. Green, T. Back, P. Natsev, and Others, "The kinetics human action video dataset," arXiv preprint arXiv:1705.06950 (2017).
42. S. Abu-El-Haija, N. Kothari, J. Lee, P. Natsev, G. Toderici, B. Varadarajan, and S. Vijayanarasimhan, "Youtube-8m: A large-scale video classification benchmark," arXiv preprint arXiv:1609.08675 (2016).
43. T. Xue, B. Chen, J. Wu, D. Wei, and W. T. Freeman, "Video enhancement with task-oriented flow," International Journal of Computer Vision **127**, 1106–1125 (2019).
44. A. Vaswani, N. Shazeer, N. Parmar, J. Uszkoreit, L. Jones, A. N. Gomez, Ł. Kaiser, and I. Polosukhin, "Attention is all you need," Advances in Neural Information Processing Systems **2017-Decem**, 5999–6009 (2017).
45. W. Shi, J. Caballero, F. Huszár, J. Totz, A. P. Aitken, R. Bishop, D. Rueckert, and Z. Wang, "Real-Time Single Image and Video Super-Resolution Using an Efficient Sub-Pixel Convolutional Neural Network," (2016).
46. M. Lu, F. W. van Tartwijk, J. Q. Lin, W. Nijenhuis, P. Parutto, M. Fantham, C. N. Christensen, E. Avezov, C. E. Holt, A. Tunnacliffe *et al.*, "The structure and global distribution of the endoplasmic reticulum network are actively regulated by lysosomes," Science advances **6**, eabc7209 (2020).
47. F. Ströhl and C. F. Kaminski, "Speed limits of structured illumination microscopy," Optics Letters **42**, 2511 (2017).
48. K. Samanta and J. Joseph, "An overview of structured illumination microscopy: recent advances and perspectives," Journal of Optics (2021).
49. Y. S. Yang and S. M. Strittmatter, "The reticulons: a family of proteins with diverse functions," Genome biology **8**, 234 (2007).